Materials for life sciences

A signal-on electrochemical aptasensor for sensitive detection of human epididymis protein 4 based on functionalized metal–organic framework/ketjen black nanocomposite

Rongqin Hu[1], Zhaode Mu[2,1], Feng Gong[3], Min Qing[2], Yonghua Yuan[1], and Lijuan Bai[1,*]

[1] *Chongqing Research Center for Pharmaceutical Engineering, College of Pharmacy, Chongqing Medical University, Chongqing 400016, People's Republic of China*

[2] *Research Center for Pharmacodynamic Evaluation Engineering Technology of Chongqing, College of Pharmacy, Chongqing Medical University, Chongqing 400016, People's Republic of China*

[3] *Chongqing Industry and Information Vocational College, Chongqing 400043, People's Republic of China*

ABSTRACT

Human epididymis protein 4 (HE4) is a highly sensitive and specific biomarker for diagnosing ovarian cancer. In this work, a new electrochemical aptasensor for rapid and sensitive detection of HE4 was constructed. Firstly, metal–organic framework/ketjen black (NH_2-MIL-53(Al)/KB) composite with abundant amino groups and large specific surface area was prepared as signal amplifier to anchor gold nanoparticles (AuNPs). Subsequently, signal probe (SP) and a large amount of electroactive toluidine blue (Tb) were attached on AuNPs to form the tracer label, producing a distinct electrochemical detection signal. Moreover, $Ni_3(HITP)_2$ was modified by poly(diallyldimethylammonium chloride, PDDA) to obtain $PDDA/Ni_3(HITP)_2$, and then it was covered with deposited gold nanocrystals (DpAu) to form the sensing platform, which increased the electrical conductivity, specific surface area and the loading of triple-helix assembled probes (TAP). Target HE4 was bound to its aptamer in the outer layer of the TAP, leaving a separate capture probe (CP) on the electrode surface that can bind with the tracer label. The proposed aptasensor for HE4 detection showed a wide linear range from 1 to 10 nM with a detection limit of 0.41 fM. In addition, the aptasensor has good selectivity, stability and reproducibility. More importantly, this method showed satisfactory results in clinical serum sample analysis compared with ELISA, possessing application prospects in ovarian cancer diagnosis.

Introduction

Ovarian cancer is a widespread malignancy that seriously threatens the health of the female reproductive system, it accounts for 4% of all cancers in women. More than 200,000 new ovarian cancer cases are diagnosed worldwide yearly [1]. Over 70% of ovarian cancer patients are diagnosed when progressing to stage II or IV [2, 3]. In addition, statistics show that 90% of patients with early diagnostic ovarian cancer can survive for more than 5 years with surgery and interventional treatment, while patients with advanced ovarian cancer that has metastasized have a 5-year survival rate of less than 30% [4]. In early diagnosis, serum tumor biomarkers are critical for patients with ovarian cancer. Although the preferred biomarkers for ovarian cancer are CA125 antigen, it has a high false positive rate and is not very sensitive for diagnosing early-stage ovarian cancer [5]. Human epididymis protein 4 (HE4) is a secreted protein of the whey acidic protein family discovered in the epithelial cells of the epididymis. The immunohistochemistry and gene microarray results showed that HE4 was not expressed in normal ovarian epithelial cells but was highly expressed in ovarian plasmacytoma and ovarian endometrioid carcinoma cells and was not expressed or lowly expressed in most non-ovarian carcinomas. According to the literature [6], the critical value of HE4 in healthy premenopausal women is 70 pM, while the value is 140 pM in postmenopausal women. Therefore, samples are generally defined as positive when their concentrations exceed 140 pM.

Currently, traditional HE4 assays mainly include enzyme immunoassay (EIA) and chemiluminescence enzyme immunoassay (CLEIA) [7]. However, these methods are prone to problems of sensitivity and accuracy. Electrochemical biosensors are widely used for their high sensitivity, simplicity, low cost and portability. For example, Mattarozzi et al. proposed a competitive immunosensing strategy to determine HE4 on magnetic microbeads with HE4 antigenic function [8]. Although antibodies have good specificity, they also have disadvantages such as higher cost and less easy preservation [9]. In recent years, aptamers, as artificially designed and synthesized single-stranded oligonucleotide fragments with strong recognition and high affinity, have been increasingly used because of their low cost, high specificity, high affinity, good stability and easy modification [10].

Nanomaterials are often applied to improve the analytical performance of electrochemical aptasensors. Metal–organic frameworks (MOFs) are of great interest because of their porosity, large surface area, structural and functional diversity, and ease of modification [11, 12]. Conductive MOFs such as Cu_3HIB_2 [13] and $Co_xNi_{3-x}(HITP)_2$ [14], are currently used in electrochemistry because of their electrical conductivity in addition to the above advantages. For example, Lei et al. prepared the complex with a conductive metal–organic framework and an ionic liquid for the detection of bisphenol A (BPA), which was supported by $Ni_3(HITP)_2$ [15]. Moreover, NH_2-MIL-53(Al) has a big aperture of 4.80 nm and an outstanding Brunauer–Emmet–Teller (BET) surface area of 187.8 m^2/g as MOF [16]. However, it has the disadvantage of poor electrical conductivity, which inhibits electron transfer [17]. Combining MOFs and carbon-based materials such as ketjen black (KB) can significantly improve the conductivity of MOFs owing to the high specific surface area, satisfactory electrical conductivity and great stability of KB [18]. Therefore, in this work, KB was combined with the MOF of NH_2-MIL-53(Al) to form the new NH_2-MIL-53(Al)/KB composite. Toluidine blue (Tb), a basic biological dye, has a special electroactivity that allows it to produce a characteristic peak in phosphate buffer. Then AuNPs are attached to the surface of NH_2-MIL-53(Al)/KB, which are used to immobilize amino groups-modified signal probe (SP) and Tb through Au–N bonds to form the tracer label.

In addition, triple-helix aptamer probe (TAP) is often used in aptasensor because of its unique structural features. TAP has the same stability and excellent affinity as double-stranded DNA [19, 20], and it requires no redesign of the probe for signal transduction, making it simple and economically efficient to operate [21]. Herein, a simple electrochemical aptasensor for HE4 was constructed. First, poly(diallyldimethylammonium chloride, PDDA) modified $Ni_3(HITP)_2$, was covered with deposited gold nanocrystals (DpAu) to form the sensing platform for the immobilization of TAP. When the target HE4 was in existence, HE4 bound to the outer loop-aptamer of the TAP immobilized on the electrode, the structure of the TAP was disrupted and the aptamer was taken away. Then the stem-capture probe (CP) inside was left exposed on the electrode and

hybridized with the added tracer label to generate a signal current for quantitative detection of HE4. Figure 1 shows the stepwise fabrication of the HE4 aptasensor and the preparation of the tracer label.

Experimental section

Materials and chemicals

N, N-dimethylformamide (DMF) and 2, 3, 6, 7, 10, 11-hexaaminotriphenylene (HATP·6HCl) were bought from Macklin Co., Ltd. (Shanghai, China). Chloroauric acid (HAuCl4), 2-aminoterephthalic acid (NH2-BDC) and poly (diallyldimethylammonium chloride) (PDDA) were ordered from Sigma-Aldrich Chemical Co. (USA). Bovine serum albumin (BSA, 98%) and toluidine blue (Tb) were brought from J&K Scientific Co., Ltd. (Beijing, China). Urea, aluminum chloride hexahydrate (AlCl3·6H2O) and nickel chloride hexahydrate (NiCl2·6H2O) were ordered from Aladdin Reagent Co., Ltd (Shanghai, China). Ethanol, ammonia water (NH3·H2O) and methanol were provided by Chongqing Chuandong Chemical Group

Co., Ltd. (Chongqing, China). Sodium citrate dihydrate was provided by Chengdu Kelong Chemical Reagent (Chengdu, China). Ketjen Black (KB) was achieved from Guangdong Canrd New Energy Technology Co., Ltd. (Guangdong, China). Human epididymis protein 4 (HE4, purity: > 95%, molecular weight: 11 kDa) was obtained from Abcam (Britain). Other chemicals were of analytical purity. The nucleotides involved were purchased by Sangon Biotech Co., Ltd (Shanghai, China) and the specific sequences are as follows:

HE4 binding aptamer [21]: 5'-(CH2)6-CTTCTCTTTATCGTACGACAGTCATCCTACACTCTCTTC-3'.

Signal probe (SP): 5'-NH2-(CH2)6-TTCTCTTCTTT-3'.

Capture probe (CP): 5'-NH2-(CH2)6-AAAGAAGAGAAG-3'.

Nucleotide solutions were prepared with 10 mM Tris–HCl buffer (pH 7.4) containing 50 mM KCl and 1 mM MgCl2. $[Fe(CN)_6]^{3-/4-}$ (5 mM) containing 0.1 M KCl was used to characterize each step in the cyclic voltammetry (CV) response of the aptasensor
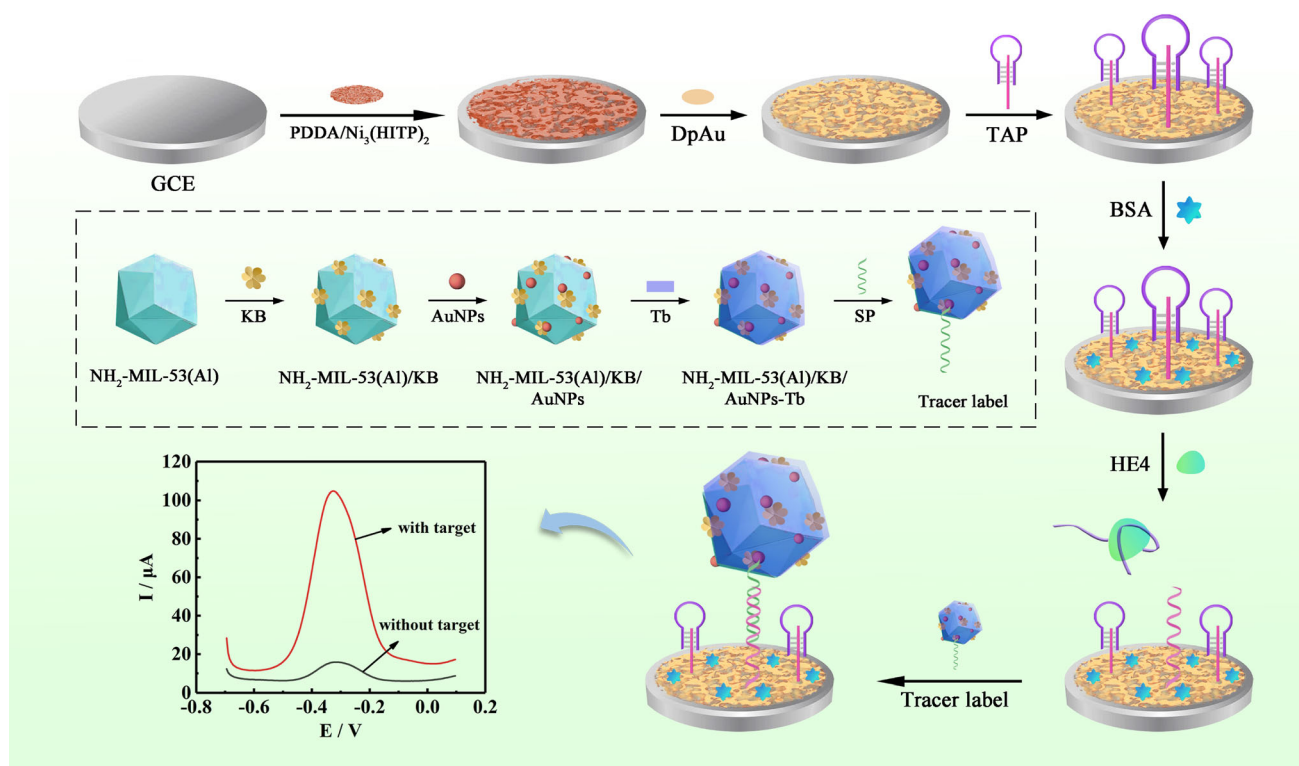

Figure 1 Schematic diagram of the preparation process of tracer label and stepwise fabrication process of the electrochemical aptasensor for HE4 (DpAu: deposited gold nanocrystals, TAP: triple-helix assembled probe, BSA: bovine serum albumin, HE4: human epididymis protein 4, KB: ketjen black, AuNPs: gold nanoparticles, Tb: toluidine blue, SP: signal probe).

and calculate specific surface area. Human serum samples were collected at the Department of Gynecology, the First Affiliated Hospital of Chongqing Medical University. This study was approved by the Ethics Committee of Chongqing Medical University (approval No. 2021109). Phosphate buffer (PB, 0.1 M, pH 7.4) containing $MgCl_2$ (2 mM) and KCl (10 mM) was used to record the differential pulse voltammetry (DPV) response of the aptasensor.

Apparatus

A three-electrode system was used for electrochemical detection, i.e., platinum wire (auxiliary electrode), modified glass carbon electrode (GCE, 4 mm in diameter, working electrode) and saturated calomel electrode (SCE, reference electrode). The measurements by CV (measurement range: $-$ 0.2 V–0.6 V with a scan rate of 100 mV s^{-1} in 5 mM [Fe(CN)$_6$]$^{3-/4-}$), DPV (measurement range: $-$ 0.7 V–0.1 V in 0.1 M PB) and electrochemical impedance spectroscopy (EIS, frequency range: 0.1 Hz to 0.1 MHz in 5 mM [Fe(CN)$_6$]$^{3-/4-}$) were made on a Metrohm Autolab electrochemical workstation (PGSTAT302N, China). Morphological and dimensional characterizations of the synthesized nanomaterials were performed by transmission electron microscopy (TEM, FEI talos f200s) and scanning electron microscope (SEM, ZEISS SIGMA 500). energy dispersive spectrometer (EDS, bruker xflash 6130, Germany), X-ray photoelectron spectroscopy (XPS, Thermo ESCALAB 250Xi, USA) and fourier transform infrared spectrometer (FT-IR, Nicolet iS 5 FT-IR, USA) were used to investigate the composition and chemical bonding properties of nanomaterials, respectively.

Preparation of PDDA/Ni (HITP)$_2$

The synthesis of Ni$_3$(HITP)$_2$ was derived from a previous literature report [15]. 38.48 mg of NiCl$_2$·6H$_2$O was dissolved in 2.38 mL of ultrapure water, and another 58.15 mg of HATP·6HCl was dispersed in 16.67 mL of ultrapure water. The above two solutions were mixed and 0.54 mL of concentrated NH$_3$·H$_2$O was applied dropwise, then stirred continuously at 60 °C for 1 h, followed by 2 h at room temperature. After the reaction, some black precipitates were obtained, washed by centrifugation three times, and then the products were dried in a vacuum oven at 25 °C for 12 h. Next, 1.5 mg of prepared Ni$_3$(HITP)$_2$

was dissolved in 1 mL of ultrapure water, and 200 μL of 1% PDDA was added subsequently and stirred overnight. After being washed by centrifugation, PDDA/Ni$_3$(HITP)$_2$ was dispersed in 1 mL of ultrapure water.

Synthesis of NH$_2$-MIL-53(Al)

NH$_2$-MIL-53(Al) was prepared based on the literature report [22]. 1.449 g of AlCl$_3$·6H$_2$O and 1.087 g of NH$_2$-BDC were dissolved in 30 mL of ultrapure water and mixed well with stirring for 30 min. Then 30 mL of ultrapure water containing 0.7205 g of urea was added dropwise with stirring for 30 min. The resulting homogeneous product was moved into the Teflon autoclave and the reaction was carried out at 150 °C for 5 h. After washed and centrifugation at 8000 rpm, the obtained composite was sequentially redissolved in DMF and methanol and stirred separately for one day. Finally, after removing the solvent by centrifugation, the obtained product was dried in oven.

Preparation of the tracer label

2 mg NH$_2$-MIL-53(Al) powder was dissolved into 2 mL ultrapure water, then 2 mg of KB was added to the dispersion, followed by sonicating until the mixture was well dispersed and then stirring gently overnight. Then 1 mL of AuNPs was added directly and stirred for 6 h. After washing by centrifugation with water, the precipitate was dissolved with 2 mL of ultrapure water to get NH$_2$-MIL-53(Al)/KB/AuNPs. Subsequently, 2 mg of Tb was added to the product obtained above, stirred for 12 h and washed several times by centrifugation. The tracer label was obtained by adding excessive SP (2 μM) and stirring gently at 4 °C for 12 h, centrifuging and dispersing in 2 mL ultrapure water.

Fabrication of the electrochemical aptasensor

First, bare GCE was initially polished with 0.3 and 0.05 μm alumina powder, and then sonication in ultrapure water and ethanol several times. After that, 10 μL PDDA/Ni$_3$(HITP)$_2$ suspension was dropped onto the mirrored surface of GCE. Continuous electrochemical deposition (potential: $-$ 0.2 V) was performed to obtain the DpAu layer. Then it was

incubated with 10 µL of prepared TAP (2 µM of aptamer and CP were mixed, heated at 95 °C for five minutes, and then incubated at 37 °C for two hours to form TAP) overnight at room temperature. Afterward, 10 µL BSA (1 wt%) was dropped on the modified electrode for 40 min to block the nonspecific sites. Finally, 20 µL of different concentrations of target HE4 and 10 µL of prepared tracer label were incubated on the electrode surface for 1.5 and 2 h, respectively. After each step, the electrodes are rinsed with DEPC water.

Results and discussion

Characterization of different materials

SEM and TEM were performed to investigate the morphological and dimensional characteristics of the as-prepared composites. $Ni_3(HITP)_2$ exhibited flower and thorn-like morphology and rough surface [23] (Fig. 2A, D). As indicated in Fig. 2B, NH_2-MIL-53(Al) had irregularly blocky structure and many spherical KB (Fig. 2C) were visibly distributed on the surface of NH_2-MIL-53(Al), indicating that NH_2-MIL-53(Al)/KB were successfully synthesized. In addition, Fig. 2E, F showed the TEM and EDS images for NH_2-MIL-53(Al)/KB/AuNPs-Tb, further confirming the synthesis of the nanohybrid.

Structural characterization of the nanocomposites

The FT-IR spectra in Fig. 3A verified the different structures of the nanomaterials and their interactions. The characteristic band of NH_2-MIL-53(Al) was seen in curve a, which was consistent with previous reports. Specifically, the two absorption peaks near 1583 and 1498 cm^{-1} represented carbonyl asymmetric stretching, while the absorption peaks around 1440 and 1401 cm^{-1} attributed to carbonyl symmetric stretching. And the bands at 3495 and 3386 cm^{-1} were due to the NH_2 group [24]. KB had no remarkable infrared absorption (curve b). There was a slight red shift (curve a) compared to NH_2-MIL-53(Al)/KB (curve c), especially the red shift of the C–H bend in the aromatic ring at 773 cm^{-1}, indicating the existence of van der Waals interactions between KB and MOF caused by C-H–π or π–π [25, 26]. Moreover, XRD pattern of Fig. 3B showed that all the

peaks of the prepared NH_2-MIL-53 were consistent with peaks of the XRD pattern in the literature [22]. Furthermore, XPS was used to illustrate the elemental composition of the NH_2-MIL-53(Al)/KB/AuNPs-Tb. As shown in Fig. 3C, it was evidenced that this nanocomposite was successfully constructed from the characteristic peaks of O1s, N1s, C1s, S2p, Au4f and Al2p.

Electrochemical characterization of the prepared HE4 aptasensor

Figure 4A showed the CV measurements in 5 mM $[Fe(CN)_6]^{3-/4-}$, which was utilized to verify the modification steps of the aptasensor. When bare GCE (curve a) was modified with $PDDA/Ni_3(HITP)_2$ (curve b) and followed by electrodeposition of DpAu (curve c), the peak current responses were increased, respectively, due to their conductive properties. When TAP was immobilized on the electrode through the Au–N bond, the current dropped due to its obstruction of electron transfer (curve d). The current response further decreased by blocking the nonspecific binding sites with nonconductive BSA (curve e). However, there was a slight increase in current due to the decrease in resistance caused by HE4 taking away the aptamer from the outer layer of the TAP (curve f). The EIS measurements on different modified electrodes were used as another tool to characterize the variation in the interfacial properties (Fig. 4B), which can respond to changes in electron transfer resistance. It can be seen that the EIS characterizations correspond to the CV measurements, suggesting the successful construction of the aptasensor.

CV was also strongly related to the specific surface area of electrodes, which reflected the properties of the substrate material. CV measurements were performed at different scan rates on bare GCE (Fig. 4C) and the $DpAu/PDDA/Ni_3(HITP)_2/GCE$ (Fig. 4E). The effective surface area of the bare GCE was calculated to be 0.086 cm^2 (Fig. 4E) from the Randle–Sevcik equation [27]. In comparison, the effective surface area of the $DpAu/PDDA/Ni_3(HITP)_2/GCE$ was 0.320 cm^2 (Fig. 4F). This demonstrated that the nanocomposite can improve the specific surface area of electrodes to promote electronic transport.
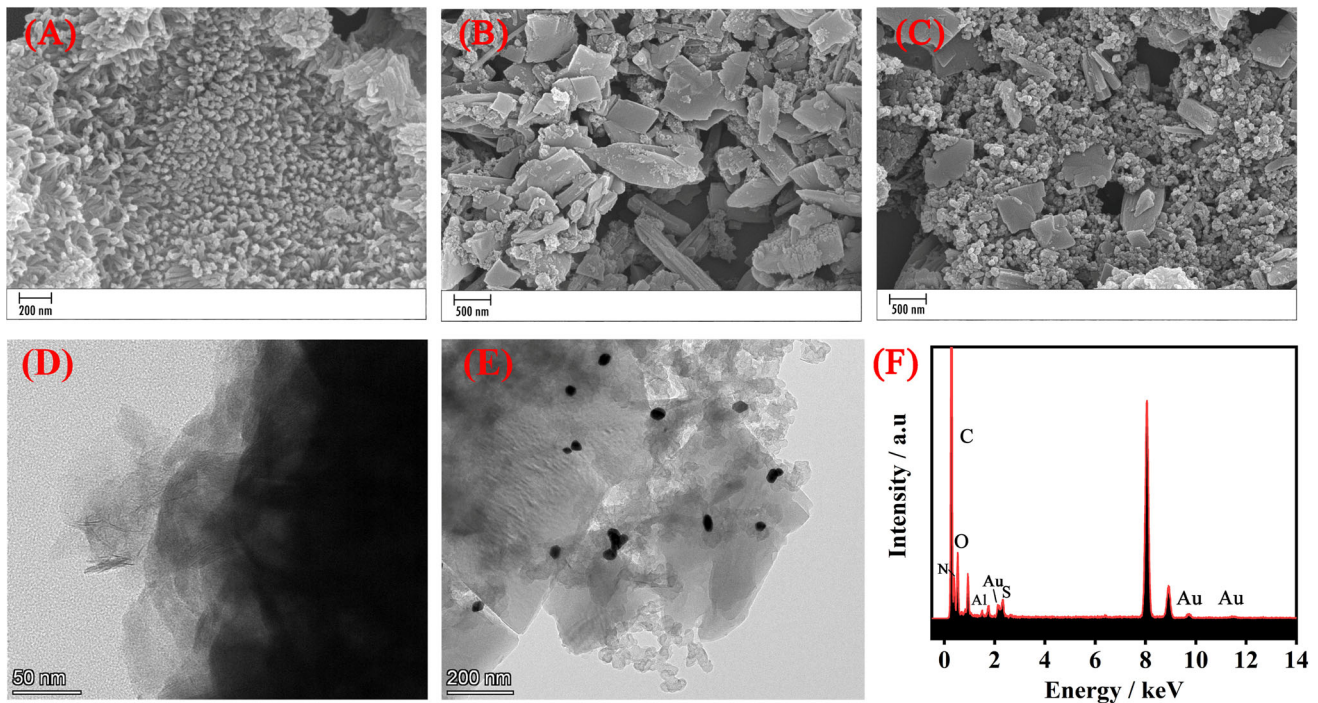
Figure 2 The SEM images of **A** $Ni_3(HITP)_2$, **B** NH_2-MIL-53(Al) and **C** NH_2-MIL-53(Al)/KB. The TEM images of **D** $Ni_3(HITP)_2$ and **E** NH_2-MIL-53(Al)/KB/AuNPs-Tb. **F** The EDS image of NH_2-MIL-53(Al)/KB/AuNPs-Tb.
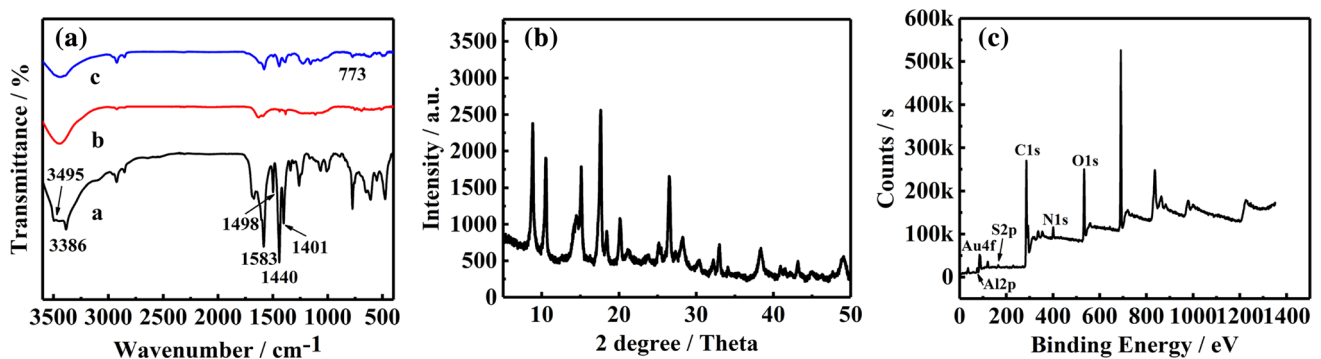

Figure 3 **A** FT-IR spectra of **a** NH_2-MIL-53(Al), **b** KB and **c** NH_2-MIL-53(Al)/KB. **B** XRD patterns of NH_2-MIL-53. **C** XPS characterizations of NH_2-MIL-53(Al)/KB/AuNPs-Tb.

Optimization of experimental parameters

The optimal NH_2-MIL-53(Al)/KB concentration ratio had significant effect on the loading amount of Tb and affected the signal response of the aptasensor. Different ratios for NH_2-MIL-53(Al)/KB were measured (NH_2-MIL-53(Al): KB = X:1, X = 0, 0.25, 0.5, 1, 2, 4). As observed in Fig. 5A, the current value reached its maximum value when the material was uniformly dispersed at a ratio of 1: 1. The response value of X = 0.25 was slightly smaller than that of X = 0 due to the poor conductivity of MOF. However,

the current increased with increased NH_2-MIL-53(Al), indicating a synergistic effect between NH_2-MIL-53(Al) and KB. However, after X exceeds 1, the current gradually decreased, mainly because the excessive MOF hindered electron transfer.

Figure 5B showed the detection of HE4 (100 fM) with DPV at 0.1 M PB of different pH levels (5, 6, 7, 7.4, 8 and 9). Since the aptamer is DNA biomolecule, and the pH of normal human blood is about 7.35 to 7.45, under highly acidic and alkaline conditions, the body's buffering system is disrupted and the
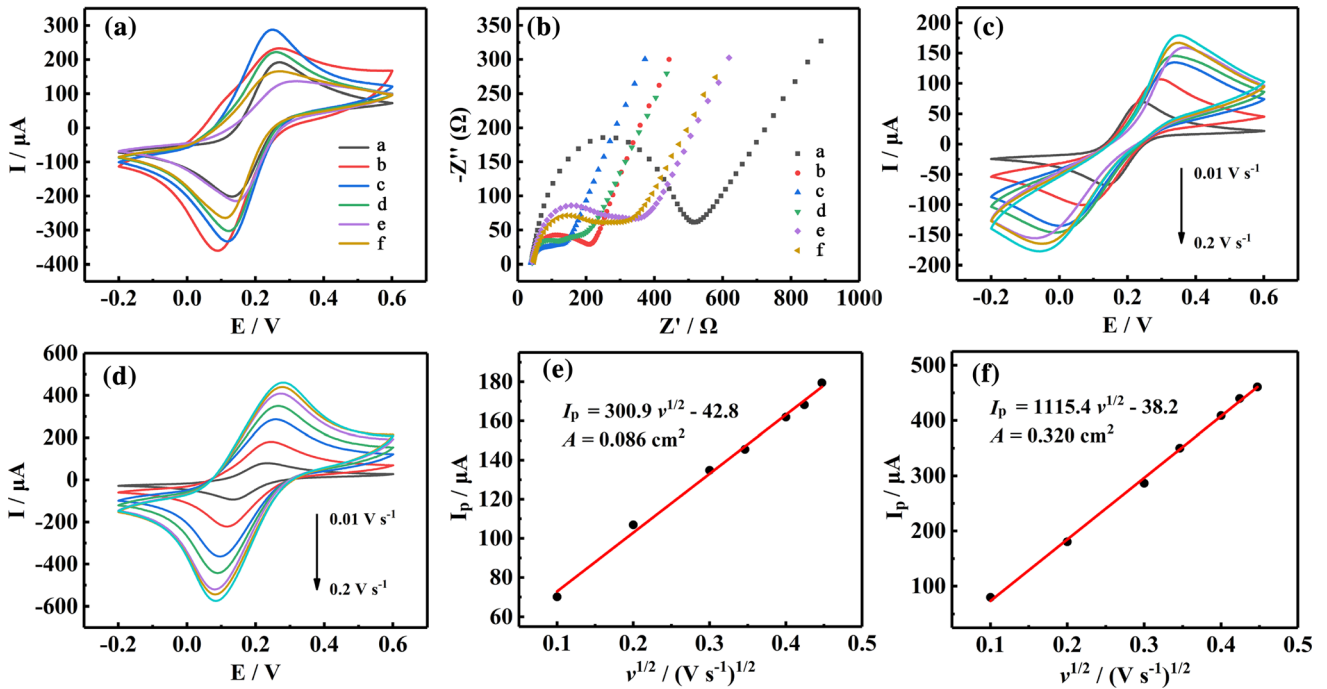
Figure 4 A CV and **B** EIS of characterization in 5 mM [Fe(CN)$_6$]$^{3-/4-}$ containing 0.1 M KCl: **a** bare GCE, **b** PDDA/Ni$_3$(HITP)$_2$/GCE, **c** DpAu/PDDA/Ni$_3$(HITP)$_2$/GCE, **d** TAP/DpAu/PDDA/Ni$_3$(HITP)$_2$/GCE, **e** BSA/TAP/DpAu/PDDA/Ni$_3$(HITP)$_2$/GCE and **f** HE4/BSA/TAP/DpAu/PDDA/Ni$_3$(HITP)$_2$/GCE. CV measurements of **C** bare GCE, **D** DpAu/PDDA/Ni$_3$(HITP)$_2$/GCE in 5 mM [Fe(CN)$_6$]$^{3-/4-}$ containing 0.1 M KCl (scan rates: 10 mV s^{-1} to 200 mV s^{-1}). The linear regression of the anodic peak currents against the square root of scan rate: **E** bare GCE, **F** DpAu/PDDA/Ni$_3$(HITP)$_2$/GCE.

Figure 5 Effect of **A** concentration ratio of NH$_2$-MIL-53(Al): KB, **B** pH of PB, **C** incubation time of HE4 and **D** time for electrodeposited DpAu.
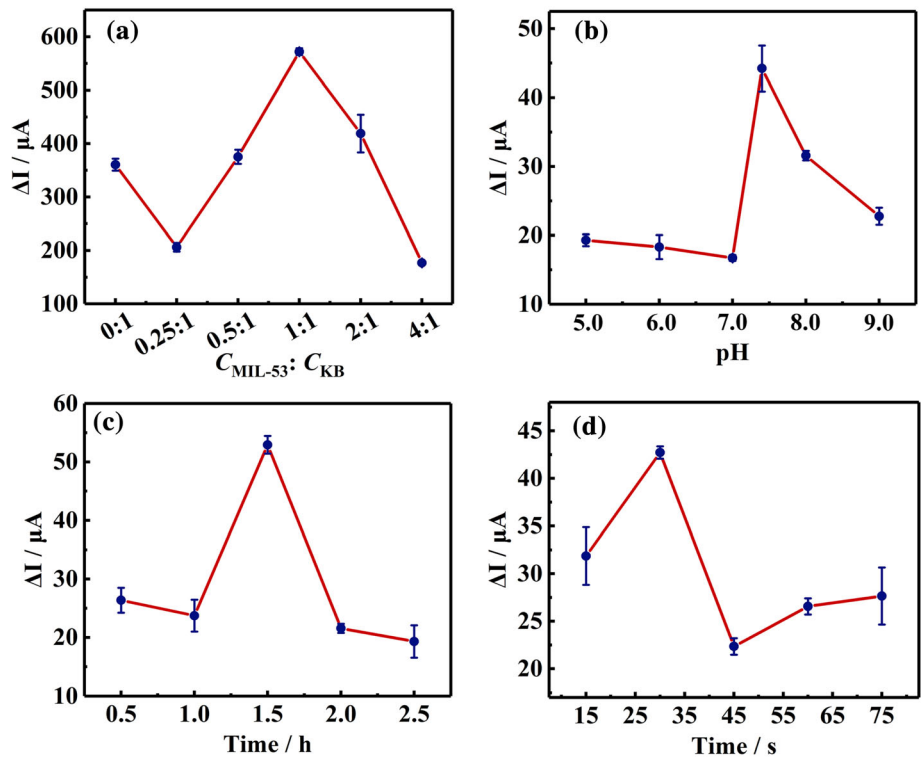
structure of nucleotides is affected. Therefore, current values have an abrupt change at about pH of 7.4.

In addition, the grafting time between CP and tracer label was also a critical factor affecting the response signal of the aptasensor and incubating the target HE4 on the electrode at different reaction times (0.5, 1.0, 1.5, 2.0 and 2.5 h). As seen in Fig. 5C, the optimal time was 1.5 h because longer reaction time will lead to the oversaturation of the protein and inhibit electron transfer.

Finally, the electrodeposition time of $HAuCl_4$ was related to the surface area for the fixed TAP and also affects the magnitude of the current response. Figure 5D shows the electrodeposition of DpAu on the electrode surface at different times (15, 30, 45, 60 and 75 s), and the maximum current value was 30 s.

Analytical performance evaluation of the aptasensor

Under optimal experimental conditions, electrochemical detection signals for different concentrations of HE4 were recorded by DPV to investigate the sensitivity and quantitative range. Figure 6A showed a good linear range of the aptasensor (1 fM to 10 nM) with a progressive increase in peak current with increasing HE4 concentration. The calibration plot was illustrated in Fig. 5B, which showed that the aptasensor has good linearity and the regression equation obtained was $\Delta I = 13.85 \lg c + 22.98$ with a correlation coefficient of 0.9985. The calculated limit of detection (LOD) was 0.41 fM. Moreover, the detection performances of the prepared aptasensor were evaluated in comparison with other previously reported methods for detecting HE4 (Table 1). It was observed that the proposed electrochemical aptasensor had wider linear range and lower LOD than that of other methods.

Stability, specificity and reproducibility studies

The short-term stability of the aptasensor was verified by continuous CV measurements on the prepared electrodes (Fig. 7A). After 50 cycles, the peak oxidation current value decreased by 8.8% compared to the initial peak oxidation current. Next, to verify long-term stability, the as-prepared aptasensors were kept at 4 °C and measured every 4 days (Fig. 7B). After 8 days and 16 days, the current remained at 92.56% and 88.64% of the initial current, respectively. It can be demonstrated that the aptasensor exhibited acceptable stability.

Since HE4 is present in human serum, where interfering substances may be present, the results were evaluated using neuron-specific enolase (NSE), human epidermal growth factor receptor 2 (HER2), human serum albumin (HSA), cytokeratin fragment antigen 21–1 (CYFRA21-1), prostate-specific antigen (PSA), carcinoembryonic antigen (CEA) and blank solution to assess the specificity of this aptasensor. As displayed in Fig. 7C, the signal of the target HE4 (10 pM) was significantly higher than the interfering substances (1 nM). At the same time, no significant difference was observed between the interferents and the blank control, indicating that these interferents did not bind significantly to the aptamer. Furthermore, the reproducibility was studied with DPV using five different electrodes prepared under the same conditions to detect 10 pM HE4 (Fig. 7D). These electrodes exhibited close current peaks with calculated RSD of 2.55%. These results showed the
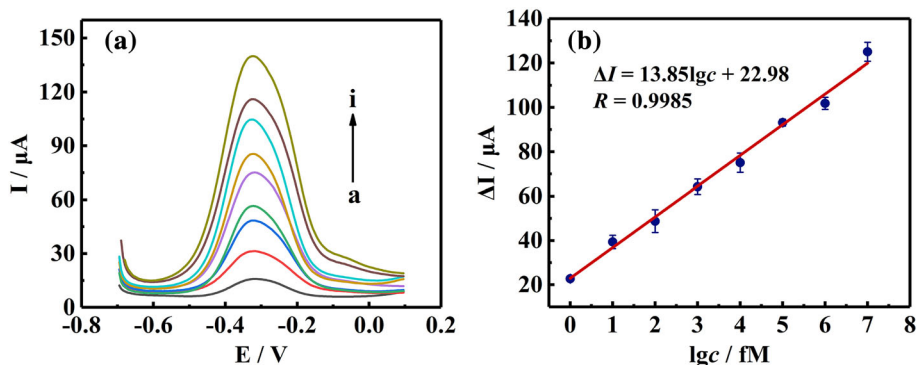

Figure 6 **A** The DPV response of aptasensor with different concentrations of HE4 was detected in 0.1 M PB (pH 7.4) (measurement range: − 0.7 V to 0.1 V). **B** Calibration curve between log HE4 concentration and current response. Error bars = SD (*n* = 3).

Table 1 Performance comparison with other methods for detecting HE4

Detection method	Recognition elements	Linear range	LOD	References
Square wave voltammetry	Antibodies	4 pM $\sim$ 400 pM	6.8 fM	[28]
Square wave anodic stripping voltammetry	Antibodies	20 pM $\sim$ 40 nM	12 pM	[29]
Localized surface plasmon resonance	Antibodies	10 pM $\sim$ 10,000 pM	4 pM	[30]
Chemiluminescence immunoassay	Antibodies	0 pM $\sim$ 1000 pM	1.35 pM	[31]
Photoelectrochemistry	Molecular imprinting polymers	0.025 $\sim$ 4 ng mL^{-1}	15.4 pg mL^{-1}	[32]
Electrochemiluminescence	Antibodies	10 fg mL^{-1} $\sim$ 10 ng mL^{-1}	3.3 fg mL^{-1}	[33]
Differential pulse voltammetry	Antibodies	0.001 $\sim$ 100 ng mL^{-1}	0.11 pg mL^{-1}	[34]
Differential pulse voltammetry	Antibodies	1 pg mL^{-1} $\sim$ 100 ng mL^{-1}	0.302 pg mL^{-1}	[35]
Differential pulse voltammetry	Antibodies	0.1 $\sim$ 300 ng mL^{-1}	0.01 ng mL^{-1}	[36]
Differential pulse voltammetry	Aptamer	1 fM $\sim$ 10 nM	0.41 fM	This work

Figure 7 **A** Short-term stability of the aptasensor with continuously scanned for 50 CV cycles in the 0.1 M PB. **B** Long-term stability of the prepared aptasensor for 16 days of signal response changes at 4 °C. **C** Selectivity of the aptasensor with various interferences. **D** Reproducibility of aptasensor with five different electrodes.
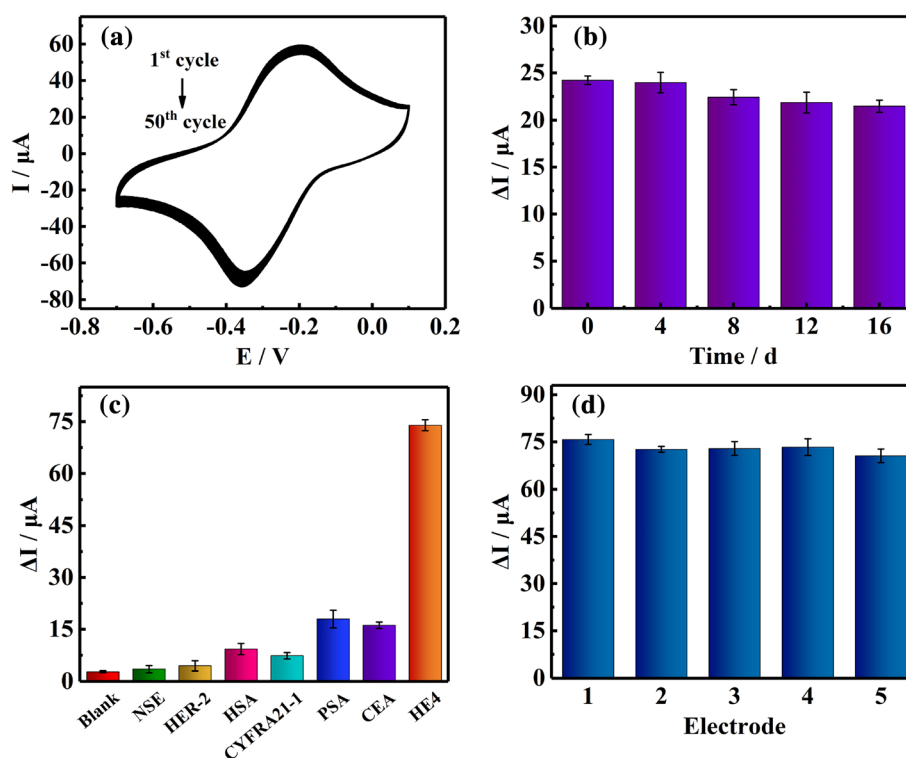
excellent selectivity and reproducibility of aptasensor for detecting HE4 within complex environments.

Recovery experiment of aptasensor

The standard addition method was used with human serum samples to further evaluate the feasibility and utility of this electrochemical aptasensor for real sample analysis. Healthy human serum samples were prepared at different concentrations of HE4 (1 fM, 100 fM, 10 pM and 1 nM) by diluting the serum samples up to 50-fold with 0.1 M PB (pH 7.4). As shown in Table 2, recovery ranged from 92.15% to 103.5% and RSD from 2.93% to 7.42%, indicating acceptable recovery of the aptasensor.

Clinical serum samples analyses

For serum samples pretreatment, they were centrifuged at 3000 rpm for 10 min and then stored in portions at − 80 °C to avoid repeated freezing and thawing to render the serum inactive (Fig. 8A). Study

Table 2 Detection of HE4 in human serum samples with the as-prepared aptasensor

Serum sample	Added HE4	Found HE4	RSD (%)	Recovery (%)
1	1 fM	1.039 fM	3.10	103.5
2	100 fM	94.52 fM	2.93	94.28
3	10 pM	9.614 pM	7.42	96.14
4	1 nM	0.9215 nM	6.73	92.15
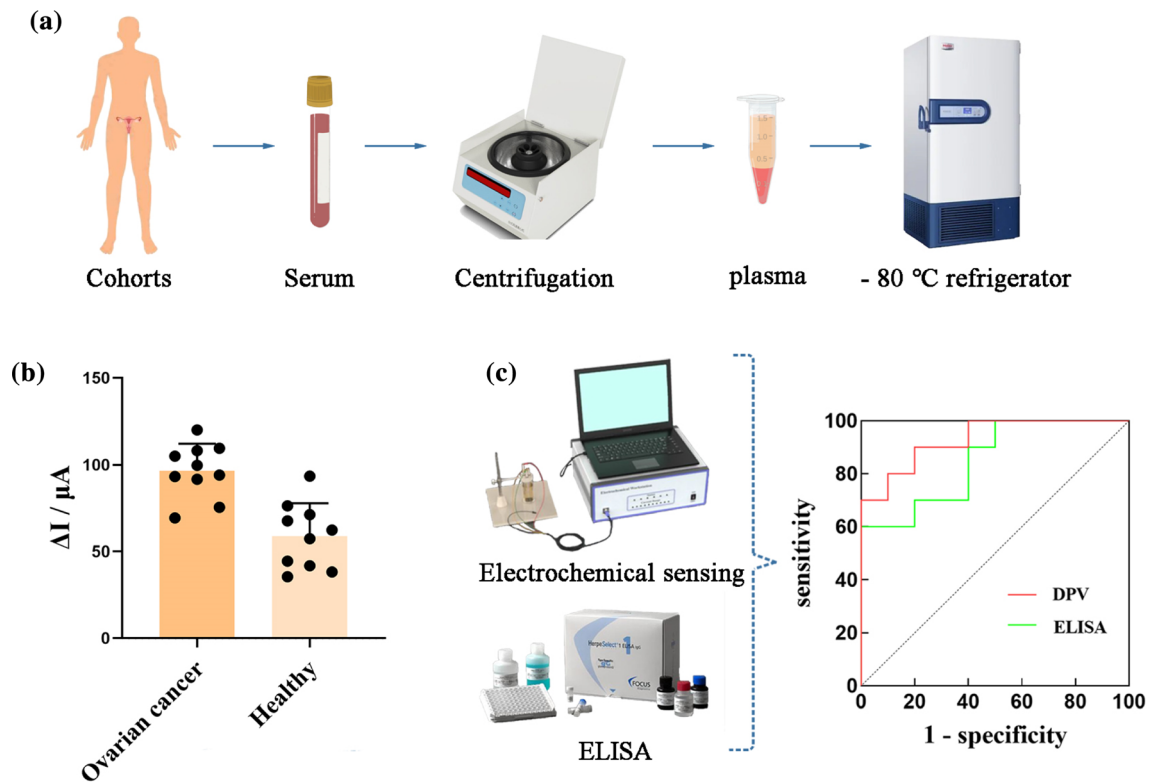
Figure 8 **A** Serum samples pretreatment. **B** DPV responses of 20 human serum samples from both ovarian cancer patients ($n = 10$) and healthy donors ($n = 10$) measured by the aptasensor, and **C** the corresponding ROC curve.

of patients with ovarian cancer ($n = 10$) and healthy volunteers ($n = 10$) of 20 human serum samples was examined to further determine the diagnostic value of the aptasensor (Fig. 8B). It was clear that the current response was higher in ovarian cancer patients than in healthy volunteers, indicating that HE4 was highly expressed in the ovarian cancer group.

Comparison of results from the aptasensor and ELISA

To evaluate the clinical application of this proposed method, 20 serum samples were tested by both aptasensors and ELISA kits. The area under the resulting ROC curve was calculated as 0.93, with a sensitivity of 90% and specificity of 80% (Fig. 8C). At the same time, the area under the ROC curve of ELISA is 0.85, which is slightly lower than that of aptasensor. These results suggest that aptasensor has great potential for clinical diagnosis of ovarian cancer. The two methods have a good correlation. Therefore, the prepared electrochemical aptasensor is expected to be a promising platform for diagnosing HE4 in human serum.

Conclusions

In summary, we have constructed an electrochemical aptasensor for HE4 detection for the first time. NH$_2$-MIL-53(Al)/KB/AuNPs-Tb nanohybrid was prepared as a new redox nanoprobe and PDDA/

Ni$_3$(HITP)$_2$ as a sensing platform to improve the detection performances of the aptasensor. As expected, NH$_2$-MIL-53(Al)/KB/AuNPs-Tb exhibited outstanding redox activity and good electrical conductivity. In addition, PDDA/Ni$_3$(HITP)$_2$ had the benefit of high specific surface area and superior electrical conductivity, which contributed to the synergistic effect of the individual nanomaterials. This aptasensor showed high sensitivity and lower LOD, as well as good stability, reproducibility and specificity. It also showed good recovery in spiked sera, opening up a new avenue for detecting HE4. However, this method has inevitable imperfections, such as complicated material and construction processes. Therefore, we will strive to improve these imperfections in our upcoming endeavors.

Acknowledgements

Data availability

The data that has been used are confidential.

Declarations

Conflict of interest The authors declare that they have no known competing financial interests or personal relationships that could have appeared to influence the work reported in this paper.

Ethical approval All experiments were performed by the guidelines "Declaration of Helsinki" and was approved by the Ethics Committee of Chongqing Medical University (Approval No. 2021109).

References

[1] Quaye L, Gayther SA, Ramus SJ, Di Cioccio RA, McGuire V, Hogdall E, Hogdall C, Blaakr J, Easton DF, Ponder BA, Jacobs I (2008) The effects of common genetic variants in oncogenes on ovarian cancer survival. Clin Cancer Res 14(18):5833–5839. https://doi.org/10.1158/1078-0432.CCR-08-0819

[2] Vargas AN (2014) Natural history of ovarian cancer. Ecancermedicalscience. 8:465–465. https://doi.org/10.3332/ecancer.2014.465

[3] Chien J, Poole EM (2017) Ovarian cancer prevention, screening, and early detection: Report from the 11th biennial ovarian cancer research symposium. Int J Gynecol Cancer 27(S5):S20. https://doi.org/10.1097/IGC.0000000000001118

[4] Schummer M, Drescher C, Forrest R, Gough S, Thorpe J, Hellström I, Hellström KE, Urban N (2012) Evaluation of ovarian cancer remission markers HE4, MMP7 and Mesothelin by comparison to the established marker CA125. Gynecol Oncol 125(1):65–69. https://doi.org/10.1016/j.ygyno.2011.11.050

[5] Rosen DG, Wang L, Atkinson JN, Yu Y, Lu KH, Diamandis EP, Hellstrom I, Mok SC, Liu J, Bast RC (2005) Potential markers that complement expression of CA125 in epithelial ovarian cancer. Gynecol Oncol 99(2):267–277. https://doi.org/10.1016/j.ygyno.2005.06.040

[6] Wu L, Dai Z-Y, Qian Y-H, Shi Y, Liu F-J, Yang C (2012) Diagnostic value of serum human epididymis protein 4 (HE4) in ovarian carcinoma: a systematic review and meta-analysis. Int J Gynecol Cancer 22(7):1106. https://doi.org/10.1097/IGC.0b013e318263efa2

[7] Ferraro S, Borille S, Carnevale A, Frusciante E, Bassani N, Panteghini M (2016) Clinical chemistry and laboratory medicine. Verifi Harmon Human Epididymis Protein 4 Assays 54(10):1635–1643. https://doi.org/10.1515/cclm-2015-1142

[8] Mattarozzi M, Giannetto M, Careri M (2020) Electrochemical immunomagnetic assay as biosensing strategy for determination of ovarian cancer antigen HE in human serum. Talanta 217:120991. https://doi.org/10.1016/j.talanta.2020.120991

[9] Wang J, Song J, Zheng H, Zheng X, Dai H, Hong Z, Lin Y (2019) Application of NiFe nanotubes as catalytically promoted sensing platform for ratiometric electrochemiluminescence analysis of ovarian cancer marker. Sens Actuators B Chem 288:80–87. https://doi.org/10.1016/j.snb.2019.02.099

[10] Kang Y, Feng K-J, Chen J-W, Jiang J-H, Shen G-L, Yu R-Q (2008) Electrochemical detection of thrombin by sandwich

approach using antibody and aptamer. Bioelectrochemistry 73(1):76–81. https://doi.org/10.1016/j.bioelechem.2008.04.024

[11] Masoomi MY, Morsali A, Dhakshinamoorthy A, Garcia H (2019) Mixed-metal MOFs: Unique opportunities in metal–organic framework (MOF) functionality and design. Angewandte Chemie Int Edition. 58(43):15188–15205. https://doi.org/10.1002/anie.201902229

[12] Kahn JS, Freage L, Enkin N, Garcia MAA, Willner I (2017) Stimuli-responsive DNA-functionalized metal-organic frameworks (MOFs). Adv Mater 29(6):1602782. https://doi.org/10.1002/adma.201602782

[13] Stassen I, Dou J-H, Hendon C, Dincă M (2019) Chemiresistive sensing of ambient CO2 by an autogenously hydrated Cu3(hexaiminobenzene)2 framework. ACS Central Sci 5(8):1425–1431. https://doi.org/10.1021/acscentsci.9b00482

[14] Song Y, Xu M, Liu X, Li Z, Wang C, Jia Q, Zhang Z, Du M (2021) A label-free enrofloxacin electrochemical aptasensor constructed by a semiconducting CoNi-based metal–organic framework (MOF). Electrochim Acta 368:137609. https://doi.org/10.1016/j.electacta.2020.137609

[15] Lei X, Deng Z, Zeng Y, Huang S, Yang Y, Wang H, Guo L, Li L (2021) A novel composite of conductive metal organic framework and molecularly imprinted poly (ionic liquid) for highly sensitive electrochemical detection of bisphenol A. Sens Actuators B: Chem 339:129885. https://doi.org/10.1016/j.snb.2021.129885

[16] Liu L, Tai X, Zhou X, Liu L (2017) Synthesis, post-modification and catalytic properties of metal-organic framework NH2-MIL-53(Al). Chem Res Chinese Univ. 33(2):231–238. https://doi.org/10.1007/s40242-017-6420-7

[17] Wang N, Zhao W, Shen Z, Sun S, Dai H, Ma H, Lin M (2020) Sensitive and selective detection of Pb (II) and Cu (II) using a metal-organic framework/polypyrrole nanocomposite functionalized electrode. Sens Actuators B Chem 304:127286. https://doi.org/10.1016/j.snb.2019.127286

[18] Grande L, Paillard E, Hassoun J, Park J-B, Lee Y-J, Sun Y-K, Passerini S, Scrosati B (2015) The lithium/air battery: still an emerging system or a practical reality? Adv Mater 27(5):784–800. https://doi.org/10.1002/adma.201403064

[19] Xiong E, Li Z, Zhang X, Zhou J, Yan X, Liu Y, Chen J (2017) Triple-helix molecular switch electrochemical ratiometric biosensor for ultrasensitive detection of nucleic acids. Anal Chem 89(17):8830–8835. https://doi.org/10.1021/acs.analchem.7b01251

[20] Zhao Y, Wang Y, Liu S, Wang C, Liang J, Li S, Qu X, Zhang R, Yu J, Huang J (2019) Triple-helix molecular-switch-actuated exponential rolling circular amplification for ultrasensitive fluorescence detection of miRNAs. Analyst 144(17):5245–5253. https://doi.org/10.1039/C9AN00953A

[21] Wang Y, Yao L, Ning G, Wu Y, Wu S, Mao S, Liu GQ (2019) An electrochemical strategy for tetracycline detection coupled triple helix aptamer probe with catalyzed hairpin assembly signal amplification. Biosens Bioelectron 143:111613. https://doi.org/10.1016/j.bios.2019.111613

[22] Chen J, Xu Y, Li S, Xu F, Zhang Q (2021) Ratio fluorescence detection of tetracycline by a Eu3+/NH2-MIL-53(Al) composite. RSC Adv 11(4):2397–2404. https://doi.org/10.1039/D0RA09185E

[23] Chen H, Xiao Y, Chen C, Yang J, Gao C, Chen Y, Wu J, Shen Y, Zhang W, Li S, Huo F, Zheng B (2019) Conductive MOF-modified separator for mitigating the shuttle effect of lithium–sulfur battery through a filtration method. ACS Appl Mater Interfaces 11(12):11459–11465. https://doi.org/10.1021/acsami.8b22564

[24] Cheng X, Zhang A, Hou K, Liu M, Wang Y, Song C, Zhang G, Guo X (2013) Size- and morphology-controlled NH2-MIL-53(Al) prepared in DMF–water mixed solvents. Dalton Trans 42(37):13698–13705. https://doi.org/10.1039/C3DT51322J

[25] Sun H, Liu D, Du J (2019) Nanobowls with controlled openings and interior holes driven by the synergy of hydrogen bonding and π–π interaction. Chem Sci 10(3):657–664. https://doi.org/10.1039/C8SC03995J

[26] Deng JH, Luo J, Mao YL, Lai S, Gong YN, Zhong DC, Lu TB (2020) π-π stacking interactions: Non-negligible forces for stabilizing porous supramolecular frameworks. Sci Adv 6(2):eaax9976. https://doi.org/10.1126/sciadv.aax9976

[27] Ma L, Bai L, Zhao M, Zhou J, Chen Y, Mu Z (2019) An electrochemical aptasensor for highly sensitive detection of zearalenone based on PEI-MoS2-MWCNTs nanocomposite for signal enhancement. Anal Chim Acta 1060:71–78. https://doi.org/10.1016/j.aca.2019.02.012

[28] Čadková M, Dvořáková V, Metelka R, Bílková Z, Korecká L (2015) Alkaline phosphatase labeled antibody-based electrochemical biosensor for sensitive HE4 tumor marker detection. Electrochem Commun 59:1–4. https://doi.org/10.1016/j.elecom.2015.06.014

[29] Cadkova M, Kovarova A, Dvorakova V, Metelka R, Bilkova Z, Korecka L (2018) Electrochemical quantum dots-based magneto-immunoassay for detection of HE4 protein on metal film-modified screen-printed carbon electrodes. Talanta 182:111–115. https://doi.org/10.1016/j.talanta.2018.01.054

[30] Yuan J, Duan R, Yang H, Luo X, Xi M (2012) Detection of serum human epididymis secretory protein 4 in patients with ovarian cancer using a label-free biosensor based on localized surface plasmon resonance. Int J Nanomed 7:2921–2928. https://doi.org/10.2147/IJN.S32641

[31] Fu X, Liu Y, Qiu R, Foda MF, Zhang Y, Wang T, Li J (2018) The fabrication of magnetic particle-based chemiluminescence immunoassay for human epididymis protein-4 detection in ovarian cancer. Biochem Biophys Rep. 13:73–77. https://doi.org/10.1016/j.bbrep.2018.01.002

[32] Wang C, Ye X, Wang Z, Wu T, Wang Y, Li C (2017) Molecularly imprinted photo-electrochemical sensor for human epididymis protein 4 based on polymerized ionic liquid hydrogel and gold nanoparticle/ZnCdHgSe quantum dots composite film. Anal Chem 89(22):12391–12398. https://doi.org/10.1021/acs.analchem.7b03486

[33] Fang D, Zhang S, Dai H, Lin Y (2019) An ultrasensitive ratiometric electrochemiluminescence immunosensor combining photothermal amplification for ovarian cancer marker detection. Biosens Bioelectron 146:111768. https://doi.org/10.1016/j.bios.2019.111768

[34] Chen DN, Jiang LY, Zhang JX, Tang C, Wang AJ, Feng JJ (2022) Electrochemical label-free immunoassay of HE4 using 3D PtNi nanocubes assemblies as biosensing interfaces. Microchim Acta 189(12):455. https://doi.org/10.1007/s00604-022-05553-6

[35] Zhang Z, Xu Y, Ma B, Ma Z, Han H (2021) A novel electrochemical sensor based on process-formed laccase-like catalyst to degrade polyhydroquinone for tumor marker. Talanta 235:122736. https://doi.org/10.1016/j.talanta.2021.122736

[36] Nawaz MAH, Akhtar MH, Ren J, Akhtar N, Hayat A, Yu C (2022) Black phosphorus nanosheets/poly(allylamine hydrochloride) based electrochemical immunosensor for the selective detection of human epididymis protein 4. Nanotechnology 33(48):485502. https://doi.org/10.1088/1361-6528/ac8bd8